

# Mechanistic studies on the electron-induced degradation of polymethylmethacrylate and Kapton

Courtney P. Ennis and Ralf I. Kaiser\*

Received 9th July 2010, Accepted 30th September 2010

DOI: 10.1039/c0cp01130d

Mechanisms for the electron-induced degradation of poly(methyl methacrylate) (PMMA) and Kapton polyimide (PMDA-ODA), both of which are commonly used in aerospace applications, were examined over a temperature range of 10 K to 300 K under ultra high vacuum ( $\sim 10^{-11}$  Torr). The experiments were designed to simulate the interaction between the polymer materials and secondary electrons produced by interaction with galactic cosmic ray particles in the near-Earth space environment. Chemical alterations of the samples were monitored on line and *in situ* by Fourier-transform infrared spectroscopy and mass spectrometry during irradiation with 5 keV electrons and also prior and after the irradiation exposure *via* UV-vis. The irradiation-induced degradation of PMMA resulted in the formation and unimolecular decomposition of methyl carboxylate radicals ( $\text{CH}_3\text{OCO}^\cdot$ ) forming carbon monoxide ( $k = 4.60 \times 10^{-3} \text{ s}^{-1}$ ) and carbon dioxide ( $k = 1.29 \times 10^{-3} \text{ s}^{-1}$ ). Temperature dependent gas-phase abundances for carbon monoxide, carbon dioxide, and molecular hydrogen were also obtained for the PMMA and Kapton samples. The lower gas yields detected for irradiated Kapton were typically one or two orders of magnitude less than PMMA suggesting a higher degradation resistance to energetic electrons. In addition, UV-vis spectroscopy revealed the propagation of conjugated bonds induced by the irradiation of PMMA and indicated a decrease in the optical band gap by an increase in absorbance above 500 nm in irradiated Kapton.

## Introduction

Poly(methyl methacrylate) (PMMA) and Kapton polyimide (poly-(pyromellitic dianhydride-4,4'-oxydianiline) or PMDA-ODA) (Fig. 1) are two examples of polymers that can be utilized for various aerospace applications. The low densities ( $\rho(\text{PMMA}) = 1.19 \text{ g cm}^{-3}$  and  $\rho(\text{Kapton}) = 1.42 \text{ g cm}^{-3}$ ) of the polymers pertain to light weight materials that can reduce the mass of a spacecraft for more efficient fuel expenditure. Optically transparent PMMA, commonly referred to as acrylic glass, is a suitable substitute for silica based glasses, particularly for applications that experience sudden shock or impact.<sup>1</sup> However, due to the susceptibility of PMMA to degrade under ionizing vacuum-ultraviolet (VUV) radiation,<sup>2</sup> it is not considered for external spacecraft components. On the other hand, Kapton is often used as a control coating for exterior spacecraft surfaces due to its thermal stability and chemical resistance.<sup>3</sup> Materials layered the outer surfaces of a spacecraft are subject to harsh environmental conditions, such as exposure to ultra high vacuum (UHV:  $10^{-9}$ – $10^{-11}$  Torr<sup>4</sup>) and experiencing substantial temperature cycling. For example, the exterior surfaces of the International Space Station (ISS) fluctuate between temperature extremes of 123 and 423 K.<sup>5</sup>

Polymer materials such as PMMA and Kapton must not only withstand the mechanical demands experienced during space-flight, they must also retain their chemical integrity after exposure to high levels of radiation in these environments. In the low-Earth orbit (LEO) region (150–1000 km<sup>6</sup>), ground and

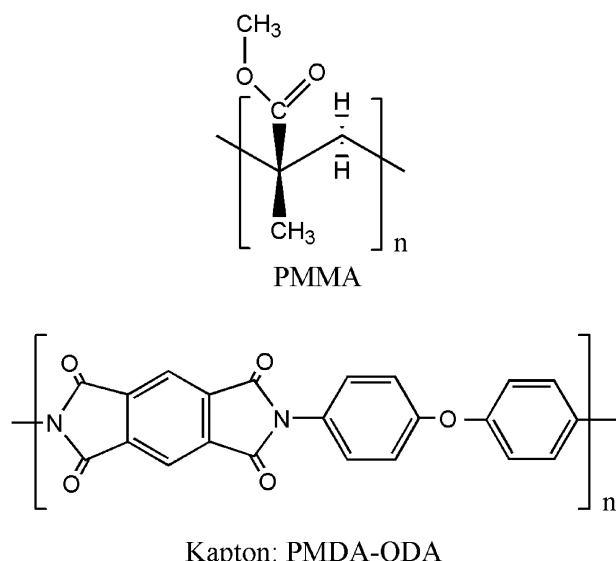


**Fig. 1** Chemical structures of poly(methyl methacrylate) (PMMA) and Kapton (poly-(pyromellitic dianhydride-4,4'-oxydianiline) or PMDA-ODA).

electronically excited atoms interact with polymers. Such particles include atomic oxygen, which at  $\sim 10^8 \text{ atoms cm}^{-3}$ <sup>7</sup> is the most abundant species in the LEO environment. Emanating from the Sun, ionizing radiation in the form of energetic ions, electrons and vacuum-ultraviolet/ultraviolet light (VUV/UV: 100–400 nm) also chemically modify the surface of a spacecraft *via* chemical degradation of the exterior material. Beyond LEO and towards the interplanetary region

Department of Chemistry, University of Hawai'i at Manoa, Honolulu, HI, 96822, USA. E-mail: ralfk@hawaii.edu

**Table 1** Selected experimental studies concerning the irradiation of poly(methacrylate) films

Reference	Thickness/nm	T/K	Pressure/Torr	Particle	Energy/eV	Products	Analytical method
Kudoh <i>et al.</i> (1996) <sup>39</sup>	$3.0 \times 10^6$	298	'vacuum'	H <sup>+</sup>	$3.0 \text{ & } 4.5 \times 10^7$	G(scission)	Mechanical testing
Ruck <i>et al.</i> (1997) <sup>40</sup>	$5\text{--}10 \times 10^3$	298	$7.5 \times 10^{-9}$	H <sup>+</sup> He <sup>+</sup>	$2.30 \times 10^5$	H <sub>2</sub> , CO, CO <sub>2</sub> C=C	QMS FTIR
Choi <i>et al.</i> (2001) <sup>41</sup>	$1.0 \times 10^4$	298	760	H <sup>+</sup>	$3.50 \times 10^5$	G(scission) decrease in FTIR C-O and C=O	FTIR Raman UV-vis
Schremppel <i>et al.</i> (2002) <sup>42</sup>	$1.0 \times 10^6$	298	760	H <sup>+</sup> He <sup>+</sup>	$10^5\text{--}10^7$	Gas evolution	Mechanical testing
Heffner (2003) <sup>26</sup>	$1.0 \times 10^6$	298	760	$\gamma$ ( <sup>60</sup> Co)	$1.17\text{--}1.33 \times 10^6$	G(scission)	FTIR
Cho & Jun (2005) <sup>43</sup>	$2.0 \times 10^6$	298	$2 \times 10^{-5}$	e <sup>-</sup>	$6.0 \times 10^4$	Surface hardening by hydrogenated amorphous carbon	Raman XPS

of space, the Galactic Cosmic Radiation (GCR),<sup>8</sup> which consists of high-energy protons (H<sup>+</sup>: 98%) and helium nuclei (He<sup>2+</sup>: 2% *i.e.*  $\alpha$ -particles), intersperse almost isotropically throughout the interstellar medium. Possessing high kinetic energies peaking at  $\sim 1$  GeV, GCR particles can easily penetrate the surface of a polymeric material lining the exterior of a spacecraft. Here, the GCR particles primarily lose kinetic energy by inelastic interaction with the surface material, generating a cascade of secondary electrons within the solid microstructure.<sup>9,10</sup> Secondary electrons can initiate breaking of chemical bonds and the generation of ionized species or radicals *via* inelastic scattering with the surrounding molecules, while lower energy secondary electrons can also attach to electron scavengers to cause bond-rupture *via* dissociative electron attachment (DEA).<sup>11</sup>

Due the importance of PMMA and Kapton in aerospace applications, many experiments investigating the exposure of these polymers to ionizing radiation have been conducted over the last decade. Utilizing a variety of experimental parameters and analytical methods, details of such studies are compiled in Table 1 and 2. In general, the PMMA and Kapton irradiation experiments were conducted at ambient temperature (298 K) and under pressures ranging from atmospheric pressure (760 Torr) to high vacuum ( $7.5 \times 10^{-9}$  Torr). In the studies involving PMMA films, irradiation with low mass particles (e<sup>-</sup>, H<sup>+</sup>, He<sup>+</sup>), possessing kinetic energies between 50 keV and 50 MeV, and gamma rays produced considerable degradation *via* chain scission and the evolution of volatile, gaseous species such as molecular hydrogen (H<sub>2</sub>), carbon monoxide (CO) and carbon dioxide (CO<sub>2</sub>). Investigations involving Kapton, which is known to be particularly resistant to ionizing irradiation, often involved irradiation with heavier atoms (Li, C and Si), possessing kinetic energies in the MeV range,

to induce degradation on the thin films (10–100  $\mu\text{m}$ ). These highly energetic interactions lead to a decrease in the optical band gap for visible light absorption observed in the UV-vis spectra collected from the irradiated Kapton samples. This was in addition to evidence of chemical alteration to the samples by way of molecular hydrogen and carbon monoxide production and the identification of new infrared absorption signals for isocyano (R-N=C=O), ketimine (R<sub>2</sub>C=N-R), and hydroxylamine groups (H-O-NR<sub>2</sub>) formed in the degraded Kapton structure.

The studies outlined above have provided a broad understanding of the degradation processes initiated in PMMA and Kapton films after exposure to highly energetic particles. However, the experimental parameters have not yet simulated the effects of secondary electrons with kinetic energies of up to the keV range as generated in the track of GCRs interacting with these polymers in the near-Earth environment. The experimental setup used in the present study simulates these interactions by irradiating the PMMA and Kapton samples with 5 keV electrons to replicate the collision energies of secondary electrons with the polymer. In addition, the near-Earth space environment is recreated in the irradiation chamber by pumping down to UHV ( $8.0 \times 10^{-11}$  Torr) pressure where experiments are conducted over a 10 K to 300 K temperature range to simulate the thermal cycling of spacecraft surfaces. Analysis of the polymer degradation processes will be conducted *in situ* by the on-line monitoring of the solid-state polymer samples by FTIR spectroscopy and in the gas-phase by mass spectrometry continuously over the three hour electron irradiation period. In addition, transmission UV-vis spectroscopy will be performed to investigate any irradiation induced changes to the optical properties of the films.

**Table 2** Selected experimental studies concerning the irradiation of Kapton films

Reference	Thickness/nm	T/K	Pressure/Torr	Particle	Energy/eV	Products	Analytical method
Virk <i>et al.</i> (2001) <sup>30</sup>	$7.5 \times 10^4$	298	$10^{-4}$	C <sup>5+</sup>	$7.0 \times 10^7$	Decrease in optical band gap	FTIR UV-vis XRD
Sun <i>et al.</i> (2002) <sup>31</sup>	$2.5 \times 10^4$	298	...	Si <sup>+</sup>	$3.0 \times 10^6$	Decrease in optical band gap	FTIR UV-vis
Sharma <i>et al.</i> (2005) <sup>34</sup>	$7.0 \times 10^4$	298	$10^{-4}$	Li <sup>3+</sup>	$5.0 \times 10^7$	CO and H <sub>2</sub> release	FTIR SEM
Li <i>et al.</i> (2007) <sup>3</sup>	$3.0 \times 10^4$	298	$10^{-5}$	H <sup>+</sup>	$3.0\text{--}10.0 \times 10^4$	Isocyano (-N=C=O), ketimine (C=C=N-) and hydroxylamine (C-O-N) groups	FTIR UV-vis
Iwata (2008) <sup>44</sup>	$2.0 \times 10^4$	413	$2.6 \times 10^{-4}$	H <sup>+</sup>	$3.0 \times 10^7$	Decrease in optical band gap	UV-vis
Li <i>et al.</i> (2008) <sup>45</sup>	$3.0 \times 10^4$	298	$10^{-5}$	H <sup>+</sup>	$9.0 \times 10^4$	Bond breaking of carbonyl and aromatic ether, ring opening of cyclic imide	AFM Raman XPS

## Experimental

Polymer film samples of PMMA (0.05 mm) and Kapton (0.008 mm) were obtained from Goodfellow Corporation (US). The samples were cut and placed on a polished silver wafer with a facial area of  $31.75 \times 31.75$  mm. The silver substrate with the polymer sample was then attached to the rotating cold-head of a closed cycle helium refrigerator (CTI-Cryogenics CP-1020) which was vertically suspended in the experimental chamber. The chamber was then evacuated to UHV conditions ( $8 \times 10^{-11}$  Torr) using an oil-free magnetically suspended turbo pump backed with an oil-free scroll pump. The experimental chamber including mounted polymer sample were heated at 320 K for a period of 24 h to removed residual gases from the sides of the chamber and from the polymer surface. During the cooling of the sample, the temperature of the cold-head was observed to reach  $11.9 \pm 0.5$  K, measured by a silicon diode sensor (Lakeshore DT-470) connected to a temperature control unit (Lakeshore 331). The use of the temperature control unit with a  $50\Omega$  cartridge heater enabled the sample temperatures to be held at 11.9, 100, 200, and 300 K during the experiments. The polymer films were then irradiated for 3 h with 5 keV electrons produced by an electron gun (SPECS EQ 22; electron extraction efficiency of 78.8%) at beam currents of 500 nA for PMMA and 5000 nA for Kapton and were scanned over a sample area of  $3.2 \pm 0.5$  cm<sup>2</sup>. The electron gun was mounted at an operating distance of 656.7 mm from the sample surface and doubly differentially pumped to maintain the UHV conditions inside the experimental chamber by preventing the migration of contaminants out-gassed by the hot filament during operation of the electron gun.

The solid-state analysis of the polymer films was performed with a Nicolet 6700 FTIR spectrometer operating in reflection mode using an external, liquid nitrogen cooled, mercury–cadmium–telluride detector. The infrared beam entered the sample at a 75° angle-of-incidence and scanned the mid-infrared (mid-IR) range of 4000–400 cm<sup>-1</sup>. The IR spectra were recorded on line and *in situ* at a resolution of 2 cm<sup>-1</sup>, with each spectrum being collected from 196 individual scans. The detection of gaseous species in the experimental chamber was performed with a quadrupole mass spectrometer (QMS) (Balzer QMG 420) operating in residual gas analyzer mode (electron impact energy of 100 eV at a 0.3 mA emission current). During a typical experiment, each polymer sample was cooled to a predetermined temperature for electron irradiation over a period of 3 h. Upon completion, the samples were left for 30 min to allow for the stabilization of any chemical or physical processes at the macro-molecular level. Each sample was then heated to 300 K (at a rate of 0.5 K minute<sup>-1</sup>) by a controlled heating program. This enabled the identification of any volatile products at their specific sublimation point under the experimental conditions. Finally, the polymer films were removed from UHV chamber for analysis with a Thermo Scientific Evolution 300 UV-vis spectrometer. Samples were mounted in the spectrometer cavity under ambient conditions for measurement in both transmission and reflection modes. Both modes scanned a spectral range of 190–1100 nm at a resolution of 1 nm.

## Results

### Irradiation conditions

The penetration depths for the impinging electrons into the polymer samples are calculated to be  $540 \pm 5$  nm for PMMA and  $480 \pm 5$  nm for Kapton using the CASINO Monte Carlo program.<sup>12</sup> This program simulates the kinetic energy loss of the 5 keV electrons *via* interaction with a polymer material of specific density and chemical composition; the results were obtained after averaging over 100 000 electron trajectories. Additional calculations are conducted to determine the average energy supplied by the impinging electrons to each polymeric monomer subunit over the 3 h irradiation period. Firstly, the total number of monomer units exposed to the electron irradiation is calculated by determining the volume of the polymer sample affected by the incident electron beam. This volume is defined by the product of the electron irradiation cross-sectional area,  $A$  (3.2 cm<sup>2</sup>) and the electron penetration depth,  $d$ , for the specific polymer. Subsequently, the total number of monomer subunits ( $\sum_{\text{monomer}}$ , in molecules) is calculated by eqn (1). Here,  $\rho$  is the density of the polymer,  $N_a$  is Avogadro's number, and  $M_m$  is the molecular mass of the monomer unit.

$$\sum_{\text{monomer}} = A \times d \times \rho \times N_a / M_m \quad (1)$$

The total energy,  $E(e^-)$  in eV, supplied by the electron irradiation to the polymer is then calculated using eqn (2), where  $I$  is the emission current of the electron gun (1.0  $\mu$ A for PMMA and 5.0  $\mu$ A for Kapton),  $E_k$  is the electron energy (5 keV),  $F$  is the electron extraction efficiency of the source ( $F = 0.788$ ),  $t$  is the irradiation time ( $1.08 \times 10^4$  s), and  $e$  is the elementary charge ( $1.60 \times 10^{-19}$  C). This gives an absorbed  $E(e^-)$  of  $8.50 \pm 0.43 \times 10^{20}$  eV for PMMA and  $4.25 \pm 0.21 \times 10^{21}$  eV for Kapton over the period of irradiation.

$$E(e^-) = I \times E_k \times F \times t/e \quad (2)$$

It follows that eqn (1) and (2) can be combined to calculate the average dose (eV molecule<sup>-1</sup>) of energy absorbed by each polymeric monomer unit (eqn (3)). These values are calculated to be  $6.87 \pm 1.37 \times 10^2$  eV molecule<sup>-1</sup> for PMMA and  $1.24 \pm 0.25 \times 10^4$  eV molecule<sup>-1</sup> for Kapton. In comparison to the typical carbon–hydrogen bond, which is about 4.5 eV strong, the considerably large dose absorbed by each polymeric monomer unit has the potential to induce substantial damage to the polymer samples.

$$\text{Dose} = E(e^-) / \sum_{\text{monomer}} \quad (3)$$

### Poly(methyl methacrylate)

**Infrared spectroscopy.** The analysis of the IR spectrum for pristine PMMA films is complicated for a number of reasons. Firstly, the PMMA samples used in the current experiments are isotactic where the methyl and methyl carboxylate functional groups on sequential monomer units are positioned on a common side of the polymer backbone. This leads to a helical PMMA structure about the carbon chain axis. This extends the number of monomer units in the PMMA unit cell for point-group analysis<sup>13</sup> and, therefore, the number of

normal vibrational modes leading to IR absorption bands in the experimental spectra. In addition, commercial PMMA generally displays a semi-crystalline physical state. This further enriches the absorption spectra as perturbation of the PMMA vibrational modes is increased by the random interactions between neighboring polymer chains in amorphous regions. These effects are dependent on the temperature of the polymer and also the production technique, where the cold-drawing process used to create the PMMA films in the present study would lend to anisotropic polymer arrangement in the direction of the stretching.

Fig. 2(top) displays the mid-IR region ( $4000\text{--}400\text{ cm}^{-1}$ ) for a PMMA film sample at 10 K. Spectra are shown for the pristine sample, after 1 h of 5 keV electron irradiation and after the irradiated 10 K sample was heated to 300 K. Averaged peak positions for the current experiments are summarized in Table 3, where they are compared with absorption bands previously assigned in the literature.<sup>14</sup> Electron irradiation experiments were also conducted at 100, 200, and 300 K, however, as the positions of the absorption bands for the higher temperature samples correlate with those produced for the 10 K investigations, spectra for these experiments are not presented. In the higher frequency region of the spectra, the intense C–H symmetric and asymmetric stretching peaks are located between  $2844$  and  $3022\text{ cm}^{-1}$ . This region contains absorption bands attributed to the  $\nu(\text{C–H})$  stretching vibrations of the methyl carboxyl and chain methyl pendent groups, as well as the main chain methylene ( $\text{CH}_2$ ). In a semi-crystalline polymer microstructure, the C–H vibrational modes on the pendent groups are influenced by neighboring polymer chains, resulting in a broad, ill-defined absorption

feature in the reflection-IR spectra. Positioned at  $1752\text{ cm}^{-1}$ , the intense absorption band associated with the carboxyl  $\nu(\text{C=O})$  stretching vibration is distinctive and in good agreement with the literature.<sup>14</sup> At frequencies below  $1500\text{ cm}^{-1}$ , the experimental spectra are observed to become totally saturated with intense absorption bands. This convoluted region contains strong absorption features associated with the various  $\delta(\text{C–H})$  deformation modes of methyl sub-units between  $\sim 1500$  and  $1350\text{ cm}^{-1}$ , the  $\nu(\text{C–O–C})$  stretching vibration of the methyl carboxyl group between  $\sim 1260$  and  $1150\text{ cm}^{-1}$  and skeletal  $\nu(\text{C–C})$  vibrations between  $\sim 1190$  and  $1150\text{ cm}^{-1}$ . However, in the  $1000\text{--}400\text{ cm}^{-1}$  region, absorption features attributed to  $\gamma_r(\text{C–H})$  rocking modes appear to be more distinct. Finally, the appearance of an absorption band at  $3440\text{ cm}^{-1}$ , in the region typically associated with  $\nu(\text{O–H})$  stretching vibrations, is unusual considering the chemical structure of pristine PMMA does not contain this identity. After consultation with the manufacturer, the absorption band could be derived from a butyl-acrylic elastomer added to the industrial polymer sample to increase impact strength.

Fig. 2 (bottom) shows the  $2500\text{--}2000\text{ cm}^{-1}$  mid-IR spectra for PMMA, recorded at 1 h intervals during the 5 keV electron irradiation period. The spectrum of the pristine film and the spectrum recorded after the heating of the PMMA sample to 300 K is also included. The PMMA samples exposed to 5 keV electrons produced two new absorption bands centered at  $2134$  and  $2338\text{ cm}^{-1}$ . These two absorption bands are identified as they are positioned in a ‘window’ between strong absorption features displayed by the pristine sample and also appear clearly above the baseline interference pattern of the thin-film. These bands are observed to increase rapidly in absorption intensity during the first hour of irradiation before leveling off at an intensity of  $\sim 0.1$  absorption units for the final two hours of irradiation. Furthermore, the absorption bands diminish in intensity during the controlled heating of the sample from 10–300 K, with the  $2134$  and  $2338\text{ cm}^{-1}$  features observed to disappear completely at sample temperatures corresponding to 230 K and 191 K respectively. The  $2134\text{ cm}^{-1}$  absorption band can be confidently assigned to the formation of solid-state carbon monoxide in the irradiated PMMA sample by identification of its  $2134\text{ cm}^{-1}$   $\nu(\text{C}\equiv\text{O})$  stretching fundamental.<sup>15</sup> Similarly, the  $2338\text{ cm}^{-1}$  absorption band can be assigned to the formation of solid-state carbon dioxide by identification of its  $2338\text{ cm}^{-1}$   $\nu(\text{O=C=O})$  asymmetric stretching mode.<sup>15</sup> These two absorption bands are the only new features observed in the mid-IR spectra for electron irradiated PMMA at 10 K, as any lower frequency features formed during the irradiation are masked by the crowded and intense mid-IR signature of the pristine PMMA film below  $1500\text{ cm}^{-1}$ . Carbon monoxide and carbon dioxide are also identified in the spectra obtained from the PMMA sample irradiated at 100 K but are absent from the higher 200 and 300 K spectra as these experiments were conducted above sublimation temperatures of the species.

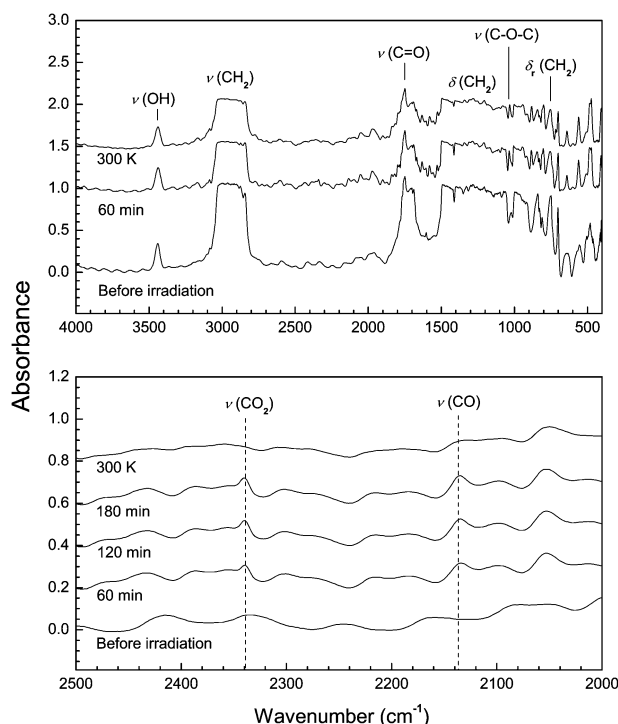


**Fig. 2** Mid-IR spectra of a PMMA film irradiated with energetic electrons for 3 h at 10 K before being heated to 300 K. The peak assignments are compiled in Table 3.

**Mass spectrometry.** For the current series of experiments investigating the 5 keV electron irradiation of PMMA films at 10 to 300 K, only QMS signals attributed to ions of molecular hydrogen ( $m/z = 2$ ), carbon monoxide ( $m/z = 28$ ) and carbon

**Table 3** Vibrational assignments of PMMA

Absorption/cm <sup>-1</sup>	Irradiation absorption/cm <sup>-1</sup>	Literature value <sup>a</sup> /cm <sup>-1</sup>	Assignment <sup>a</sup>	Characterization <sup>a</sup>
406		406	$\nu(C-C)$	C–C stretch
482		484	$\gamma_r(CH_2)$	CH <sub>2</sub> rock
571		559	$\gamma_r(CH_2)$	CH <sub>2</sub> rock
652		...		
704		...		
751	802	757	$\nu(C-C)$	C–C stretch
812		810		
840	883	843	$\gamma_r(CH_2)$	CH <sub>2</sub> rock
910–999		966–989	$\gamma_r(O-CH_3)$	O–CH <sub>3</sub> rock
1027	1038	...		
1059–1401		1193 and 1150 1273 and 1242 1387 and 1367	$\nu_a(C-O-C)$ $\nu_s(C-C-O)$ $\delta_s(CH)$ of $\alpha$ -CH <sub>3</sub>	C–O–C asym. stretch C–C–O sym. Stretch C–H deformation
1426–1496		1436 1448 1485	$\delta_s(CH)$ of O–CH <sub>3</sub> $\delta_a(CH)$ of $\alpha$ -CH <sub>3</sub> $\delta(CH_2)$	C–H deformation C–H deformation C–H deformation
1604				
1711				
1752	2134 2338	1750 2135 <sup>b</sup> 2340 <sup>b</sup>	$\nu(C=O)$ $\nu(CO)^b$ $\nu_3(CO_2)^b$ $\nu(C-H)$	Carbonyl stretch CO <sup>b</sup> CO <sub>2</sub> <sup>b</sup> C–H stretching
2844–3022		2841–3029		
3084				
3443			$\nu(O-H)$	O–H stretching

<sup>a</sup> Dybal and Krimm 1990; <sup>b</sup> Bennett 2009.

dioxide ( $m/z = 44$ ) displayed an increase in their abundances during the 3 h irradiation period. Surprisingly, the ion counts for methane and other higher mass hydrocarbons likely to be created by the decomposition of PMMA (including their associated electron impact fragment species) did not appear to increase in abundance. Fig. 3 displays the ion counts of singly ionized molecular hydrogen ( $H_2^+$ ) generated over the course of the experiments. For sample temperatures between 100 and 300 K, the peak  $H_2^+$  current occurs immediately after the onset of the electron exposure ( $t = 0$  min) before displaying an exponential-like decay over time. The current is then observed to drop to the background level of the blank

experiment after completion of the irradiation ( $t = 180$  min). The peak  $H_2^+$  current displays some correlation to the temperature of the irradiated PMMA sample. At 300 K, the peak ion current is measured to be  $2.45 \times 10^{-11}$  A, close to an order of magnitude higher than the  $4.5 \times 10^{-12}$  and  $3.8 \times 10^{-12}$  A peak currents recorded for the 200 K and 100 K experiments respectively. However, in the  $H_2^+$  profile recorded at 10 K, the peak current is not detected until 20 min into the heating period. Corresponding to a molecular hydrogen sublimation temperature of  $\sim 20$  K, the  $H_2^+$  ion current is observed to increase to  $2.0 \times 10^{-12}$  A after being released from the polymer sample.

Fig. 4 displays the  $CO^+$  and  $CO_2^+$  ion counts that are recorded for the 10 and 100 K experiments (top) and for the 200 and 300 K experiments (bottom). The low ion currents detected for both  $CO^+$  and  $CO_2^+$  species during the irradiation period ( $t = 0$ –180 min) infer that the 10 K experiments are performed below the sublimation points for both species. Likewise, in the 100 K experiments, the carbon monoxide might diffuse very slowly from the bulk to the surface. For example, the 100 K experiment yields  $CO^+$  and  $CO_2^+$  ion currents of  $1.7 \times 10^{-11}$  A and  $1.1 \times 10^{-11}$  A respectively at the start of irradiation. However, as the controlled heating of the PMMA is initiated, a significant increase in ion current for both species is observed as the temperature is increased to 300 K and the volatile species are out-gassed from the PMMA sample. The  $CO^+$  ion count for the 10 K experiment reaches a maximum current of  $8.1 \times 10^{-11}$  A at 90 K, while the 100 K experiment reaches a maximum current of  $7.3 \times 10^{-11}$  A at 140 K. Furthermore, the 100 K experiment produces the highest  $CO_2^+$  ion current at 165 K ( $2.5 \times 10^{-11}$  A) while

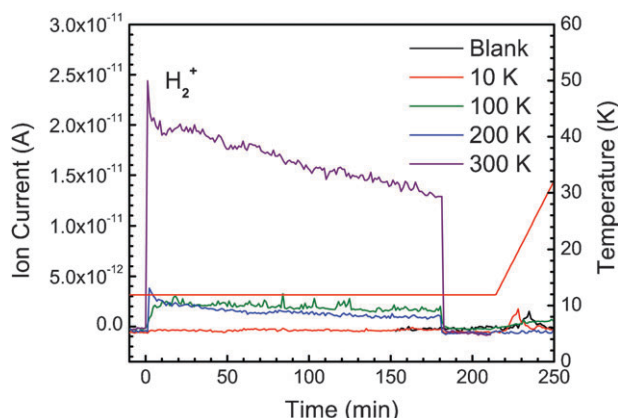


**Fig. 3** Ion count for singly ionized molecular hydrogen ( $H_2^+$ ) released from PMMA films irradiated with energetic electrons at 10, 100, 200 and 300 K over the 3 h irradiation period. Temperature increase for the controlled heating of the 10 K sample is also depicted.

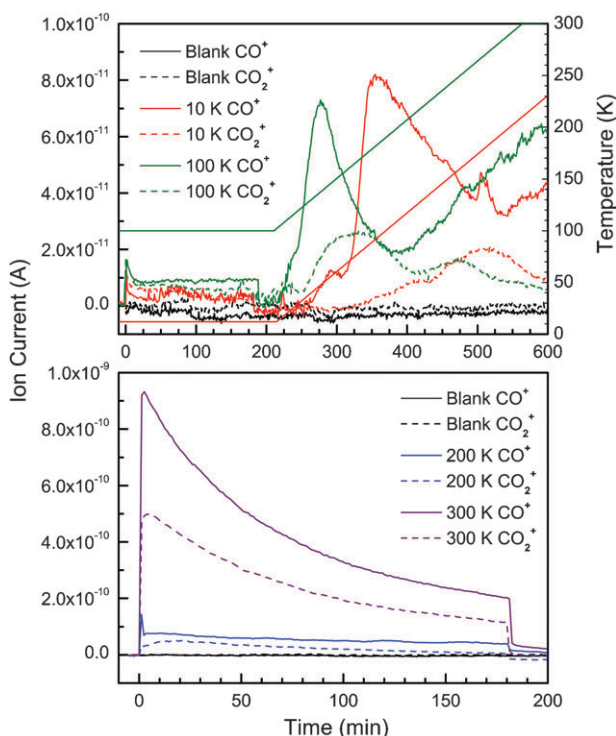


**Fig. 4** Ion count for singly ionized carbon monoxide ( $\text{CO}^+$ ) and carbon dioxide ( $\text{CO}_2^+$ ) released from PMMA films irradiated with energetic electrons at 10, 100, 200 and 300 K over the 3 h irradiation period. Temperature increase for the controlled heating of the 10 and 100 K samples are also depicted.

the maximum  $\text{CO}_2^+$  ion current recorded for the 10 K experiment corresponds to a sublimation temperature of 180 K ( $2.0 \times 10^{-11}$  A).

For the experiments conducted at higher sample temperatures (Fig. 4, bottom), the ion counts for the  $\text{CO}^+$  and  $\text{CO}_2^+$  species return to the baseline level after irradiation is completed at  $t = 180$  min. This indicates complete out-gassing of any product carbon monoxide and carbon dioxide during the exposure period. The temperature dependence displayed for the lower temperature experiments is upheld, with the 300 K sample producing  $\text{CO}^+$  and  $\text{CO}_2^+$  ion currents of  $9.4 \times 10^{-10}$  A and  $5.0 \times 10^{-10}$  A respectively at  $t = 0$  min. The peak currents recorded for the 200 K sample is approximately an order of magnitude smaller, with  $\text{CO}^+$  producing a maximum ion current of  $1.4 \times 10^{-10}$  A and  $\text{CO}_2^+$  a maximum ion current of  $6.2 \times 10^{-11}$  A. After the peak ion currents are detected at the onset of irradiation, the ion profiles for both  $\text{CO}^+$  and  $\text{CO}_2^+$  are observed to decrease in an exponential-like decay until the electron exposure is stopped ( $t = 180$  min), after which the detected current returns back to the baseline level.

**UV-vis spectroscopy.** Fig. 5 displays the transmission UV-vis spectra recorded for the series of electron irradiation experiments performed on PMMA films. The spectrum of a pristine PMMA film is also included for comparison. For the pristine and irradiated PMMA samples, the entire visible region ( $\lambda > 400$  nm) displays zero absorbance, which is to be expected considering the widespread use of PMMA as an

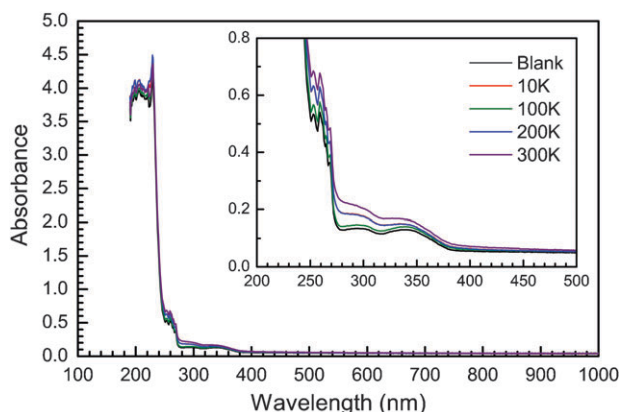


**Fig. 5** UV-vis spectra of PMMA films irradiated with energetic electrons for 3 h at 10, 100, 200 and 300 K. The blank spectrum of pristine PMMA film is also displayed.

optically transparent window material. However, the far UV limit of the experimental spectra ( $\lambda < 300$  nm) displays a strong absorbance edge produced by electronic excitations within the carboxyl ( $\text{C}=\text{O}$ ) chromophore in the PMMA structure.<sup>16</sup> The most intense absorption feature in the 200–230 nm region is attributed to the  $\pi \rightarrow \pi^*$  transitions in the  $\text{C}=\text{O}$  system while the 270–300 nm absorption feature is attributed to ‘forbidden’  $n \rightarrow \pi^*$  transitions that possess a lower absorption intensity.

Following electron irradiation, the 225–375 nm region (Fig. 5-inset) displays an increase in absorption intensity corresponding to the increased sample temperature during exposure. This is likely due to irradiation induced formation of conjugated diene ( $-\text{C}=\text{C}-\text{C}-$ ) groups through unsaturation of the PMMA chain. An increase in the density of diene groups in the sample would result in an increase in absorption over the 225–375 nm wavelength range, with the magnitude of the red-shift dependent on the number of successive diene groups formed in the polymer chain. The process of diene formation is observed to be temperature dependent from the increase in absorption from 10 to 300 K. This is due to the enhanced mobility of dissociated radical species such as atomic hydrogen at higher temperatures, preventing these reactive species from back-reacting with the newly formed  $-\text{C}=\text{C}-$  groups.

### Kapton

**Infrared spectroscopy.** Commercial Kapton of the type used in the present experiments possesses a semi-crystalline microstructure with an anisotropic chain arrangement, which is characteristic of the cold-drawing technique for thin film manufacture. Therefore, the Kapton IR spectrum is affected by both the temperature and the degree of crystallinity of the sample. In Kapton (Fig. 1), a single monomer unit represents a single unit cell containing the total number of vibrational elements leading to absorption bands in the IR spectra.<sup>17</sup> This is opposed to the complicated point group analysis required to account for the total number of vibrational modes for the helical PMMA structure discussed previously. However, the presence of various cyclic and aromatic species in a single Kapton monomer unit complicates the 1000–400  $\text{cm}^{-1}$  region

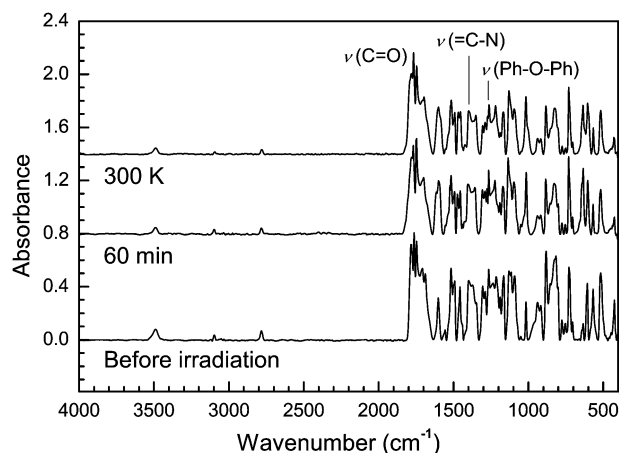


**Fig. 6** Mid-IR spectra of a Kapton film irradiated with energetic electrons for 3 h at 10 K before being heated to 300 K. The peak assignments are compiled in Table 4.

of the mid-IR spectrum, primarily because of the large number of moderately absorbing deformation modes associated with the aromatic groups.<sup>18</sup>

Fig. 6 displays the 4000–400  $\text{cm}^{-1}$  mid-IR region for Kapton film recorded during the present experiments at 10 K. The absorption band positions are compiled in Table 4 where their assignments are made by comparison to literature values.<sup>18</sup> The 0.008 mm thick Kapton samples produced significant interference patterns in the reflectance-IR absorption spectra over the entire mid-IR range and required manual baseline correction. The 5 keV (5  $\mu\text{A}$ ) electron irradiation experiments were also performed on Kapton samples held at 100, 200 and 300 K. However, the

spectra obtained at higher irradiation temperatures closely resembled the spectra recorded at 10 K and are not presented.

The strongest absorption feature in the 1850–1640  $\text{cm}^{-1}$  mid-IR region is assigned to the stretching mode carbonyl groups  $\nu(\text{C}=\text{O})$ . This feature is particularly broad as it superimposes the in-phase and out-of-phase stretching modes of the  $\text{C}=\text{O}$  groups, which oscillate at slightly different frequencies.<sup>19</sup> In addition, a lower frequency band at 636  $\text{cm}^{-1}$  is assigned to the deformation mode of the carbonyl group  $\delta(\text{C}=\text{O})$ . The imide groups contribute the 726  $\text{cm}^{-1}$  deformation band  $\delta(\text{C}-\text{N}-\text{C})$  as well as the intense, broad regions at 1118, 1165 and 1370  $\text{cm}^{-1}$  which are attributed to the stretching  $\nu(\text{C}-\text{N}-\text{C})$  vibrations of the group. The diphenylether group in the Kapton structure is assigned to the  $\nu(\text{C}-\text{O}-\text{C})$  stretching bands at 1239 and 1264  $\text{cm}^{-1}$ . Aromatic groups account for many of the remaining absorption bands in Table 3 due to their numerous lower frequency  $\delta(\text{phenyl})$  deformation modes (e.g. the 901–982  $\text{cm}^{-1}$  region). These aromatic groups also contribute  $\nu(\text{C}-\text{H})$  stretching absorption features in the 3020–3155  $\text{cm}^{-1}$  region which display only low absorption intensities.

The exposure of the Kapton films to 5 keV electrons with an irradiation current of 5.0  $\mu\text{A}$  induces some observable changes to the mid-IR spectra of the 10 K sample. Some of the low frequency absorption features display shifts in band position, possibly due to alteration of the Kapton microstructure after exposure. These changes include the imide deformation band shifting from 726  $\text{cm}^{-1}$  to 732  $\text{cm}^{-1}$  and the imide stretching band at 1118  $\text{cm}^{-1}$  being repositioned to 1135  $\text{cm}^{-1}$ . There is some precedence in the literature for swelling to occur in irradiated polymers<sup>20</sup> due to cross-link formation or for volatile species becoming trapped in the polymer microstructure,

**Table 4** Vibrational assignments of Kapton

Absorption/ $\text{cm}^{-1}$	Irradiation absorption/ $\text{cm}^{-1}$	Literature value <sup>a</sup> / $\text{cm}^{-1}$	Assignment <sup>a</sup>	Characterization <sup>a</sup>
570		568	$\delta(\text{phenyl})$	Phenyl ring deformation
607		607	$\delta(\text{phenyl})$	Phenyl ring deformation
636		636	$\delta(\text{C}=\text{O})$	Carbonyl deformation
706		705		
726	732	725	$\delta(\text{C}-\text{N}-\text{C})$	Imide deformation
755		752	$\delta(\text{phenyl})$	Phenyl ring deformation
777		776	$\delta(\text{phenyl})$	Phenyl ring deformation
788–865		825	$\delta(\text{C}-\text{H})$	Out-of-plane phenyl deformation
883		885	$\delta(\text{phenyl})$	Phenyl ring deformation
901–982		896–960	$\delta(\text{phenyl})$	Phenyl ring deformation
	1029	...		
1094		1095		
1118	1135	1117	$\nu(\text{C}-\text{N}-\text{C})$	Imide stretch
1165		1168	$\nu(\text{C}-\text{N}-\text{C})$	Imide stretch
1189		1188	$\delta(\text{phenyl})$	Phenyl ring deformation
1239		1243	$\nu(\text{C}-\text{O}-\text{C})$	Bridging C–O–C stretch
1264		1260	$\nu(\text{C}-\text{O}-\text{C})$	Bridging C–O–C stretch
	1275	...		
1288–1305		1290–1307	$\delta(\text{phenyl})$	Phenyl ring deformation
1332–1420	1383	1376	$\nu(\text{C}-\text{N}-\text{C})$	Imide stretch
1435–1570		1456–1555	$\nu(\text{phenyl})$	Phenyl ring C–C stretch
1600		1600	$\nu(\text{phenyl})$	Phenyl ring C–C stretch
	1618	...		
1640–1850		1725	$\nu(\text{C}=\text{O})$	Out-of-phase carbonyl stretch
		1779	$\nu(\text{C}=\text{O})$	In-phase carbonyl stretch
3020–3155			$\nu(\text{C}-\text{H})$	Phenyl ring C–H stretch
3488				

<sup>a</sup> Ishida *et al.* (1980).

particularly at low temperature. Subsequently, the internal modes of vibration for the Kapton molecules would become less perturbed by their neighboring counterparts, inducing shifts in the band position of certain absorbing species, in this case to slightly higher (blue-shifted) frequencies. In addition, there is some evidence for new absorption features in the 1000–1650 cm<sup>-1</sup> region of the spectra, identified at 1029, 1275 and 1618 cm<sup>-1</sup>. As these bands are of moderate absorption intensity and are all positioned within close proximity to strong absorption features associated with pristine Kapton, it is hard to conclusively assign these new bands to specific species produced *via* electron irradiation, or even assign to absorption bands shifted from their original positions by a change in the polymer microstructure. There is no evidence for new absorption bands at higher frequencies produced from the exposure of Kapton films, significantly at the 2135 and 2340 cm<sup>-1</sup> positions which are associated with carbon monoxide and carbon dioxide.

**Mass spectrometry.** The experimental QMS analysis of the Kapton films at 10 to 300 K detected an increase in the electron impact ion counts for molecular hydrogen ( $m/z = 2$ ), carbon monoxide ( $m/z = 28$ ) and carbon dioxide ( $m/z = 44$ ), after being out-gassed by the samples during the irradiation and controlled heating periods. Fig. 7 displays the ion counts for H<sub>2</sub><sup>+</sup> generated over the course of the experiments. The H<sub>2</sub><sup>+</sup> ion profiles are similar to those produced for irradiated PMMA films, where the peak ion currents for the 100–300 K experiments occur at the onset of electron exposure ( $t = 0$  min) before decaying away over the 3 h irradiation period. The 10 K experiment is observed to retain solid-state molecular hydrogen in the polymer microstructure during the 3 h irradiation period. After the sample is heated to ~20 K during the controlled heating stage, molecular hydrogen is out-gassed from the Kapton surface to yield a sharp increase in the H<sub>2</sub><sup>+</sup> ion current to  $2.35 \times 10^{-11}$  A. There appears to be little temperature dependence on gas-phase hydrogen abundance as the ion counts for the 100 and 200 K experiments are both low (maximum  $\sim 1.0 \times 10^{-12}$  A at  $t = 0$  min), compared to the significantly larger peak ion current recorded for the 300 K experiment ( $1.45 \times 10^{-11}$  A at  $t = 0$ ).

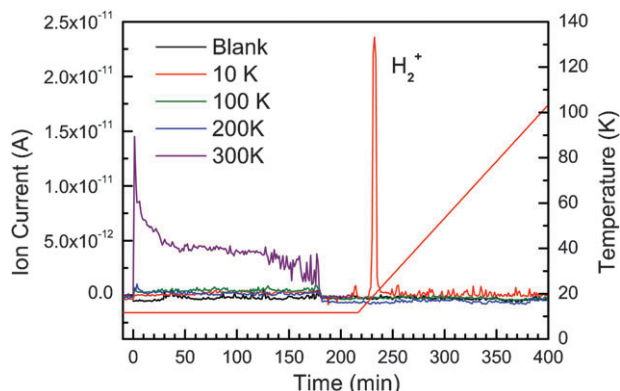


**Fig. 7** Ion count for singly ionized molecular hydrogen (H<sub>2</sub><sup>+</sup>) released from Kapton films irradiated with energetic electrons at 10, 100, 200 and 300 K over the 3 h irradiation period. Temperature increase for the controlled heating of the 10 K sample is also depicted.

The ion count profiles for CO<sup>+</sup> produced by the irradiated Kapton films are displayed in Fig. 8. For the 10 to 200 K experiments, the peak ion counts recorded at  $t = 0$  min appear to be similar at  $\sim 1.2 \times 10^{-11}$  A, while the 300 K experiment returned a significantly larger ion count of  $6.9 \times 10^{-11}$  A. Over the electron exposure period, the CO<sup>+</sup> ion counts for 10–200 K samples appeared to decrease at different rates before returning to the baseline level at  $t = 180$  min. However, the ion count for the 300 K sample was observed to fluctuate dramatically over the same exposure period, rapidly decreasing to  $1.4 \times 10^{-11}$  A at  $t = 25$  min before increasing in an exponential manner back to  $4.8 \times 10^{-11}$  A before irradiation was ceased at  $t = 180$  min. Finally, after the commencement of the heating of the sample, a considerable amount of residual carbon monoxide was observed to be out-gassed at  $t = 235$  min from the Kapton sample that was originally at 10 K. The CO<sup>+</sup> ion count at this point was  $1.75 \times 10^{-11}$  A to coincide with a sublimation temperature of 21 K.

Fig. 9 displays the ion count profiles for CO<sub>2</sub><sup>+</sup> generated by the irradiated Kapton samples. For the higher temperature experiments (100–300 K), the evolution of gas-phase carbon

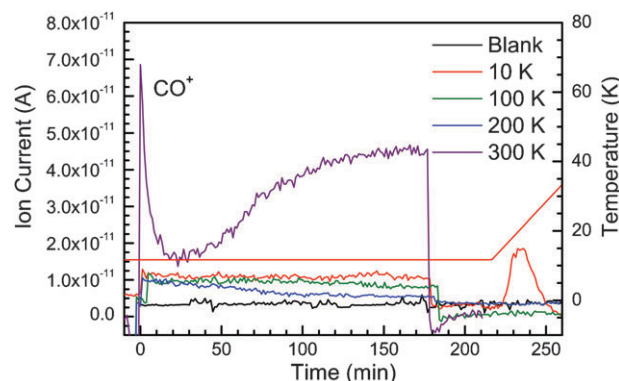


**Fig. 8** Ion count for singly ionized carbon monoxide (CO<sup>+</sup>) released from Kapton films irradiated with 5 keV electrons at 10, 100, 200 and 300 K over the 3 h irradiation period. Temperature increase for the controlled heating of the 10 K sample is also depicted.

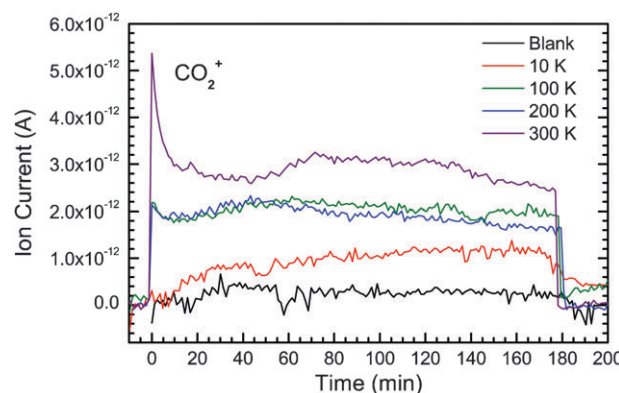


**Fig. 9** Ion count for singly ionized carbon dioxide (CO<sub>2</sub><sup>+</sup>) released from Kapton films irradiated with energetic electrons at 10, 100, 200 and 300 K over the 3 h irradiation period.

dioxide occurs early in the exposure period as the samples are irradiated above the carbon dioxide sublimation temperature. The 300 K experiment produces a peak ion current of  $5.4 \times 10^{-12}$  A at  $t = 0$  min while the 100 and 200 K experiments produce a peak ion current of  $2.2 \times 10^{-12}$  A at  $t \approx 60$  min. For these experiments, the  $\text{CO}_2^+$  ion counts appear to fluctuate over the exposure period before rapidly diminishing back to the baseline level after the irradiation is ceased at  $t = 180$  min. Surprisingly, the 10 K experiment also produces a gradual increase in the  $\text{CO}_2^+$  ion current over the 3 h irradiation period to a maximum  $1.2 \times 10^{-12}$  A at  $t \approx 160$  min. This is unexpected, as carbon dioxide is well below its sublimation temperature at 10 K. Therefore, it should be retained in the solid-state to be out-gassed only during the controlled heating stage. However, the observation of out-gassed carbon dioxide at 10 K may explain its absence in the associated IR spectrum for the 10 K experiment in Fig. 6, as there is no absorption band identified in the  $2340 \text{ cm}^{-1}$  position for the species in the solid-state.

**UV-vis spectroscopy.** The transmission UV-vis spectra of Kapton films collected after the 3 h electron irradiation at sample temperatures of 10, 100, 200, and 300 K are shown in Fig. 10, together with the spectrum for a pristine Kapton film for comparison. The saturation of the UV spectra at wavelengths lower than 400 nm is due intense absorbance features associated with  $\pi \rightarrow \pi^*$  transitions in the aromatic groups.<sup>18,21</sup> This absorbance pattern tails into the visible region, leading to the materials amber coloring. Depicted in Fig. 10 (Inset), an irradiation induced increase in absorbance is observed over the entire visible region (500–1000 nm), with a distinct absorption peak at 700 nm. This can be attributed to a decrease in the optical band gap for  $\pi \rightarrow \pi^*$  transitions. This is indicative of an overall increase in conjugated systems in the polymer microstructure. However, it is clear by the superposition of the spectra collected from the Kapton samples that there is no obvious temperature dependence for the extent of this absorbance increase.

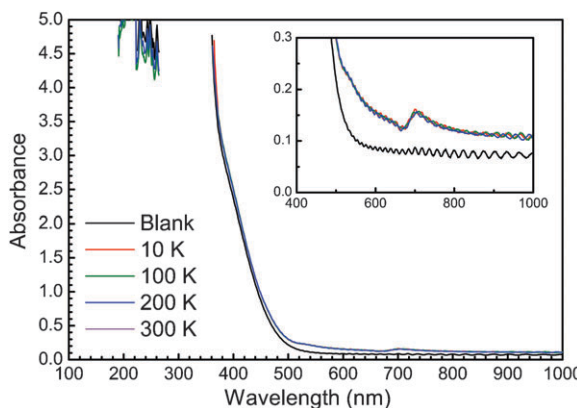


**Fig. 10** UV-vis spectra of Kapton films irradiated with energetic electrons for 3 h at 10, 100, 200 and 300 K. A blank spectrum of pristine Kapton film is also displayed.

## Discussion

### Polymer degradation

**Poly(methyl methacrylate).** Previous studies investigating the irradiation of PMMA with ionizing radiation (Table 1) have identified chain scission as a primary degradation pathway for the polymer. Generally, the chain scission process is more readily associated with polymers that have large pendant groups attached to the carbon backbone, as these provide a steric hindrance to the formation of cross-links.<sup>22</sup> A previous study<sup>23</sup> involving the exposure of PMMA to 20 keV electrons did display that cross-linking is an alternate degradation pathway to the chain scission process when using electrons of a similar energy to the 5 keV electron irradiation energy applied in the present experiments. Here, an increase in the dosage of electron irradiation produced a decrease in the solubility of the polymer, inferring that the growth of the molecular mass of the PMMA sample was due to the formation of cross-links.

The detection of cross-links in the PMMA samples is not feasible with the analytical equipment used in the present study. In addition, evidence for chain scission can not be provided *via* identification of the resultant terminal vinyl ( $-\text{CR}=\text{CH}_2$ ) groups in the FTIR spectra, as the  $910 \text{ cm}^{-1}$  absorption band<sup>2</sup> characteristic for this moiety is positioned in a region of the mid-IR spectrum that is populated by strong absorption bands associated with the pristine PMMA sample. Identification of structural alterations to the PMMA sample is limited to the observation of a temperature dependent increase in absorption intensity in the 225–375 nm region of the UV-vis spectra. This absorption increase infers an increase in density within the polymer sample of chromophores that allow  $\pi \rightarrow \pi^*$  transitions, most likely by the formation of sequential  $-\text{C}=\text{C}-$  unsaturated centers in the main chain.

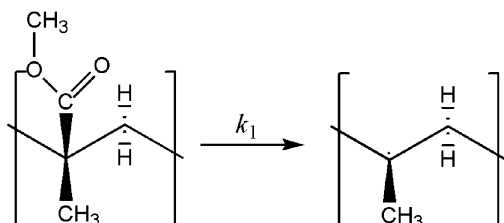
The QMS analysis of electron irradiated PMMA films indicates that a significant amount of gas-phase, molecular hydrogen, (Fig. 3) carbon monoxide and carbon dioxide (Fig. 4) is generated from the samples during the irradiation period and during the subsequent controlled heating of the samples to 300 K. Evidence is provided by an increase in the ion current detected for the  $\text{H}_2^+$ ,  $\text{CO}^+$  and  $\text{CO}_2^+$  species. Furthermore, the ion currents for these gas-phase species rise with an increase in sample temperature. The abundance of gas-phase, molecular hydrogen, carbon monoxide and carbon dioxide can be quantitatively calculated from their respective ion profiles in Fig. 3 and 4. For example, the QMS ion current (A) for  $\text{H}_2^+$  was recorded for specific pressures of hydrogen gas introduced to the main chamber. This was then calibrated by scaling the  $\text{H}_2^+$  ion current with the molecular hydrogen pumping speed of the UHV system ( $S_{\text{eff}} = 770 \text{ L s}^{-1}$ ), specific to the dimensions of the experimental chamber. The experimental molecular hydrogen pressures calculated from the integrated temporal ion current profiles were then converted to a total number of hydrogen molecules generated from the irradiated PMMA surface (Table 5). Similar calibration methods were also adopted for the calculation of carbon monoxide and carbon dioxide gas yields from the same experiments. Here, the abundance of gas-phase hydrogen

**Table 5** Gas phase abundances of species evolved from irradiated PMMA and Kapton derived *via* mass spectrometry

T/K	H <sub>2</sub> ( $\times 10^{15}$ molecules)	CO ( $\times 10^{16}$ molecules)	CO <sub>2</sub> ( $\times 10^{16}$ molecules)
PMMA			
10	0.23 ± 0.02	1.92 ± 0.13	9.47 ± 0.63
100	1.26 ± 0.08	9.26 ± 0.62	4.72 ± 0.32
200	1.36 ± 0.09	11.5 ± 0.8	7.29 ± 0.49
300	19.2 ± 1.3	25.3 ± 1.7	13.0 ± 0.9
Kapton			
10	3.59 ± 0.24	1.49 ± 0.10	1.85 ± 0.12
100	0.118 ± 0.008	8.57 ± 0.57	1.02 ± 0.07
200	0.041 ± 0.003	0.47 ± 0.03	0.89 ± 0.06
300	0.331 ± 0.022	4.41 ± 0.30	5.53 ± 0.37

was observed to be largest at 300 K ( $19.2 \pm 1.3 \times 10^{15}$  molecules), which was approximately an order of magnitude larger than the other three sample temperatures (averaged to be  $0.95 \pm 0.11 \times 10^{15}$  molecules from the 10, 100 and 200 K experiments). The yield of gas-phase carbon monoxide displayed a sample temperature dependent increase from  $1.92 \pm 0.13 \times 10^{16}$  molecules at 10 K to  $25.3 \pm 1.7$  molecules at 300 K. Carbon dioxide showed a similar increase from 100 K ( $4.72 \pm 0.32 \times 10^{16}$  molecules) to 300 K ( $13.0 \pm 0.9 \times 10^{16}$  molecules), however, the second largest yield was recorded at 10 K ( $9.47 \pm 0.63 \times 10^{16}$  molecules).

To complement the quantitative measurement of the gaseous products evolved from PMMA films irradiated with 5 keV electrons, kinetic data can be derived for the production of carbon monoxide and carbon dioxide in the solid-state by the *in situ* analysis of the FTIR spectra in Fig. 2. For the 10 K experiment which was conducted below the respective sublimation temperatures for carbon monoxide and carbon dioxide, the temporal increase in intensity of the  $\nu(\text{C}\equiv\text{O})$   $2134 \text{ cm}^{-1}$  symmetric stretching and the  $\nu(\text{O}=\text{C}=\text{O})$   $2338 \text{ cm}^{-1}$



asymmetric stretching absorption bands indicate an increase in the column density ( $\text{molecules cm}^{-2}$ ) of the species in the irradiated PMMA films. In more detail, over the 3 h irradiation period, the integrated absorption bands were converted to carbon monoxide and carbon dioxide column densities ( $\text{molecules cm}^{-2}$ ) by use of a Lambert-Beer expression, which was modified for the path of the reflected IR beam through the film samples. Literature absorption coefficients, or  $A$ -values, of  $1.0 \times 10^{-17} \text{ cm molecule}^{-1}$  for the  $2134 \text{ cm}^{-1}$  symmetric stretching band of carbon monoxide<sup>24</sup> and  $7.6 \times 10^{-17} \text{ cm molecule}^{-1}$  for the  $2338 \text{ cm}^{-1}$  asymmetric stretching band of carbon dioxide<sup>25</sup> were obtained for these calculations.

There is precedence in the literature to construct degradation mechanisms for electron induced PMMA that result in the formation of carbon monoxide and carbon dioxide.

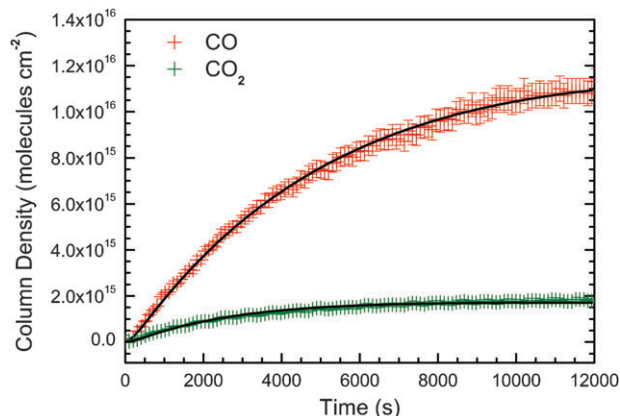
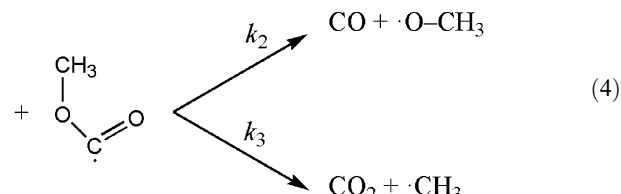


**Fig. 11** Column densities for solid-state carbon monoxide and carbon dioxide formed during the irradiation of PMMA film at 10 K over the 3 h exposure period with energetic electrons.

A previous study<sup>26</sup> investigating the exposure of PMMA samples to  $\gamma$ -irradiation has shown that the methyl carboxylate group is easily cleaved from the  $\alpha$ -carbon of the PMMA monomer (eqn (4)). If this process is taken to apply for the electron irradiation experiments conducted in the present research, the dissociated methyl carboxylate radical can undergo unimolecular decomposition inducing a C–O bond rupture to form the carbon monoxide molecule and a methoxyl radical ( $\cdot\text{O}-\text{CH}_3$ ) or a carbon dioxide molecule and a methyl radical ( $\cdot\text{CH}_3$ ). Fig. 11 displays the column densities for carbon monoxide and carbon dioxide measured during the 3 h irradiation period for the PMMA samples at 10 K. These temporal profiles were fitted with sequential (A → B → C) kinetic models (eqn (5) and (6))<sup>27</sup> to represent the irradiation induced degradation of a single PMMA monomer unit by the following reaction scheme:



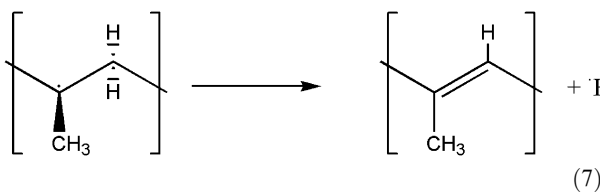
$$[\text{CO}](t) = [\text{PMMA}]_0 \left( 1 - \frac{k_2}{k_2 - k_1} e^{-k_1 t} + \frac{k_1}{k_2 - k_1} e^{-k_2 t} \right) \quad (5)$$

$$[\text{CO}_2](t) = [\text{PMMA}]_0 \left( 1 - \frac{k_3}{k_3 - k_1} e^{-k_1 t} + \frac{k_1}{k_3 - k_1} e^{-k_3 t} \right) \quad (6)$$

Here, the fitted kinetic curves are derived from the initial column density of PMMA monomer ( $[\text{PMMA}]_0 = 3.44 \times 10^{17} \text{ molecules cm}^{-2}$ ) which is converted to a degraded PMMA monomer unit and the methyl carboxylate radical reaction intermediate at a rate  $k_1 = 8.97 \times 10^{-6} \text{ s}^{-1}$ , over time,  $t$ . Subsequently, the methyl carboxylate radical can

undergo one of two unimolecular destruction pathways to result in the formation of carbon monoxide or the formation of carbon dioxide, both in the solid-state at 10 K. The fitted temporal profiles for each species calculates a rate of  $k_2 = 4.60 \times 10^{-3} \text{ s}^{-1}$  for the pathway leading to carbon monoxide (eqn (5)) and a rate of  $k_3 = 1.29 \times 10^{-3} \text{ s}^{-1}$  for the pathway leading to carbon dioxide (eqn (6)). Finally, as the column densities for carbon monoxide and carbon dioxide are observed to level off as  $t \rightarrow \infty$  (Fig. 11), destruction mechanisms for both species were added to the scheme. The destruction rate for carbon monoxide was calculated to be  $k = 1.81 \times 10^{-4} \text{ s}^{-1}$  while the destruction rate for carbon dioxide was calculated to be  $k = 3.60 \times 10^{-4} \text{ s}^{-1}$ .

We would not expect to see evidence for the methoxyl radical or methyl radical products in the mid-IR spectra as their literature solid-state vibrational frequencies<sup>28,29</sup> are in regions that are also occupied by intense absorption bands associated with the PMMA monomer. However, the radical center of the  $\alpha$ -carbon, produced by the dissociation of the methyl carboxylate group (eqn (4)), quickly forms a double bond and promotes the release of a hydrogen atom (eqn (7)).<sup>26</sup> This process, if occurring in successive monomer units on the polymer chain, increases the density of conjugated  $-\text{C}=\text{C}-$  groups, leading to the observed increase in absorption of the 225–375 nm region in the UV-vis spectrum (Fig. 5).



**Kapton.** Previous studies investigating the irradiation of Kapton films with a variety of energetic particles, under a range of experimental conditions, are summarized in Table 2. Irradiation with high LET particles commonly resulted in the UV-vis absorption spectrum shifted to longer wavelengths due to the formation of new chromophores.<sup>30,31</sup> These collisions also caused significant chemical alteration to the Kapton samples with the monomer unit appearing susceptible to bond rupture at a number of sites within its structure.<sup>32,33</sup> Carbon monoxide was commonly observed to be out-gassed during exposure at ambient conditions,<sup>34</sup> indicating the breaking of the imide ring which resulted in the decrease in intensity of the  $\delta(\text{C}-\text{N}-\text{C})$  absorption band in the FTIR spectra.<sup>35</sup>

The 5 keV electron irradiation used in the present study was not expected to degrade the Kapton samples to the degree of the high LET experiments discussed above. The FTIR spectra collected over the three hour electron exposure period (Fig. 6) did not display any new absorption features that could be confidently assigned to degradation products. This included missing spectral evidence for carbon monoxide (*i.e.*  $\nu(\text{C}\equiv\text{O})$  at  $\sim 2135 \text{ cm}^{-1}$ ) in the solid-state for the 10 K experiment. Shifts in the position of certain absorption features attributed to aromatic deformation modes ( $1275$  and  $1029 \text{ cm}^{-1}$ ) could indicate the breakdown of the Kapton monomer into its aromatic subunits, although these shifts could also indicate a change in chain conformation induced by the transfer of

irradiation energy. In addition, shifts in position of the  $\delta(\text{C}-\text{N}-\text{C})$  and  $\nu(\text{C}-\text{N}-\text{C})$  modes of the imide groups indicate they are also significantly affected by exposure to electrons. The UV-vis spectra obtained from the samples irradiated at 10–300 K in the present study (Fig. 10) did display an increase in absorption at wavelengths longer than 500 nm compared to the pristine Kapton film, suggesting an increase in the density of chromophore species in the Kapton microstructure.

However, the QMS provided the strongest evidence for chemical alteration of the irradiated Kapton films where the evolution of molecular hydrogen, carbon monoxide and carbon dioxide was identified in the gas-phase by an increase in the detectable currents of the  $\text{H}_2^+$  (Fig. 7),  $\text{CO}^+$  (Fig. 8) and  $\text{CO}_2^+$  (Fig. 9) species produced *via* electron impact ionization. Here, the only quantitative analysis of molecular hydrogen, carbon monoxide and carbon dioxide abundances could be performed. Calculations were conducted in the same manner as the irradiated PMMA films, where the detectable ion currents were scaled to the pumping speed of the experimental apparatus and a total number of molecules evolved could be measured (Table 5). These calculations produced low yields for molecular hydrogen, which is expected due to only the strongly bound aromatic hydrogen existing in the Kapton composition. The highest yield was produced after the 10 K sample was heated to the molecular hydrogen sublimation temperature at  $\sim 20$  K ( $3.59 \pm 0.24 \times 10^{15}$  molecules). This was an order of magnitude greater than the yields produced for the 100, 200 and 300 K samples during their exposure.

The total abundance of carbon monoxide and carbon dioxide out-gassed from the irradiated Kapton samples were observed to be in the order of  $10^{16}$  molecules, with no general correlation to the sample temperature observed. The highest carbon monoxide yield was recorded at 100 K ( $8.57 \pm 0.57 \times 10^{16}$  molecules) while the highest carbon dioxide yield was recorded at 300 K ( $5.53 \pm 0.37 \times 10^{16}$  molecules). Although the levels of each species is of a similar magnitude to the irradiated PMMA samples investigated previously (Table 5), the electron dosage per monomer unit for Kapton ( $1.24 \pm 0.25 \times 10^4 \text{ eV molecule}^{-1}$ ) is significantly larger than for the PMMA samples ( $6.87 \pm 1.37 \times 10^2 \text{ eV molecule}^{-1}$ ). This indicates a significant difference between radiation resistances for the PMMA and Kapton polymers to 5 keV electrons.

#### Concluding remarks on implications for PMMA and Kapton used in aerospace design

Before we discuss potential implications of our research, it is important to summarize the results of our experiments (Table 6; Fig. 12).

**Poly (methyl methacrylate).** (1) FTIR: The formation of carbon monoxide and carbon dioxide was confirmed at 10 K by the observation of the  $\nu(\text{CO})$  band at  $2134 \text{ cm}^{-1}$  and the  $\nu(\text{CO}_2)$  band at  $2338 \text{ cm}^{-1}$ . The rates of formation were calculated to be  $4.60 \pm 10^{-3} \text{ s}^{-1}$  and  $1.29 \times 10^{-3} \text{ s}^{-1}$  respectively from the unimolecular decomposition of methyl carboxylate radicals which were dissociated from the irradiated PMMA films.

(2) QMS: The evolution of molecular hydrogen, carbon monoxide and carbon dioxide could be monitored by their ion

**Table 6** Summary of irradiation induced polymer alterations

	FTIR	QMS	UV-vis
PMMA	CO & CO <sub>2</sub>	H <sub>2</sub> , CO & CO <sub>2</sub>	$\pi \rightarrow \pi^*$
Kapton	Structural alteration	H <sub>2</sub> , CO & CO <sub>2</sub>	Decrease in optical band gap > 500 nm

currents and their gas-phase abundances were determined to be independent on the temperature of the irradiated sample.

(3) UV-vis: An increase in absorption above 250 nm due to  $\pi \rightarrow \pi^*$  transitions in newly formed conjugated systems is evident.

**Kapton.** (1) FTIR: The possible identification of dissociated benzene trapped in polymer network by way of shifted  $\delta$ (phenyl) deformation bands.

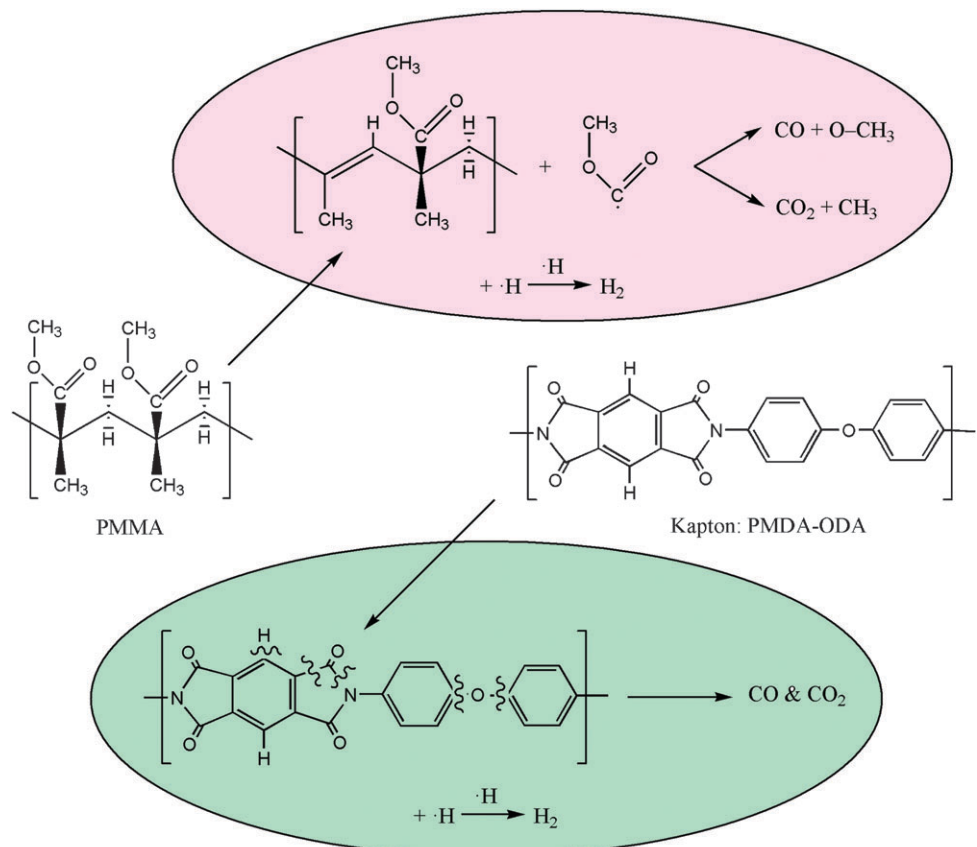
(2) QMS: The evolution of molecular hydrogen, carbon monoxide and carbon dioxide could be monitored by their ion currents and their gas-phase abundances were determined to be independent on the temperature of the irradiated sample.

(3) UV-vis: An increase in absorbance for wavelengths greater than 500 nm due to  $\pi \rightarrow \pi^*$  transitions suggesting the formation of extended conjugated  $\pi$  systems.

These results as summarized above suggest that PMMA and Kapton both degrade after exposure to 5 keV electrons to produce common products, mainly molecular hydrogen, carbon monoxide and carbon dioxide. However, the reaction

mechanisms displayed by both materials resulting in the formation of these products are unique and differ strongly. Firstly, for PMMA, the methyl carboxyl pendent group of the repeating monomer unit appears readily dissociated from the carbon backbone during irradiation (eqn (4)). Here, the methyl carboxyl group can undergo one of two pathways of unimolecular decomposition to result in either a carbon monoxide molecule and a methoxyl radical (eqn (5)) or a carbon dioxide molecule and a methyl radical (eqn (6)). In addition, the carbon radical center on the PMMA chain can form a *trans*- carbon–carbon double bond; this is connected with the release of atomic hydrogen (eqn (7)). It is also expected that the reactive hydrogen atom can easily recombine to form the molecular hydrogen species identified by QMS analysis.

The degradation mechanisms associated with irradiated Kapton films is much harder to elucidate. The formation of carbon monoxide is probably due to the dissociation of the carboxyl group of the amide ring on the repeating monomer unit. Here, it is feasible that the carbon monoxide molecule can on-react with a suprathermal oxygen atom,<sup>15</sup> which is most likely released by the cleaving of the phenyl bridging group, to result in the carbon dioxide species observed in the QMS results. Alternatively, previous investigations<sup>36</sup> of low temperature carbon monoxide ices, also irradiated with 5 keV electrons, have shown that two carbon monoxide molecules (one excited and one ground state) can react to form carbon dioxide *via* the release of a ground state carbon atom. Molecular hydrogen formation is independent of this process,

**Fig. 12** Overview of the electron induced degradation of PMMA and Kapton.

formed by way of addition of two atomic hydrogen species cleaved from irradiated phenyl groups.

For both the PMMA and Kapton samples irradiated at 10 K, the molecular hydrogen, carbon monoxide and carbon dioxide products are trapped within the polymer microstructure after formation. Upon controlled heating of the samples back to 300 K, the sublimation profiles for each species reveal information on their respective diffusion processes. The spatially small molecular hydrogen molecules are released from both PMMA and Kapton films at  $\sim$ 20 K (Fig. 3 and 7), unhindered by electrostatic interaction with the polar centers associated with both materials. However, the carbon monoxide and carbon dioxide molecules sublime over a much broader temperature range (e.g. Fig. 4: CO  $\sim$  40–100 K and CO<sub>2</sub>  $\sim$  90–180 K) than the sublimation points for pure carbon monoxide ice and carbon dioxide ice of 37 K and 90 K respectively.<sup>37</sup> This is due to the slow diffusion of carbon monoxide and carbon dioxide inside the substrate before being out-gassed. This suggests that irradiated organic polymers can build-up significant amounts of gases at least at lower temperatures.

In the context of radiation induced degradation of polymeric materials used in the harsh LEO and near-Earth space environments, these results have important implications. Extended missions like the ISS rely on polymer materials such as PMMA and Kapton for thermal control coatings and for structural applications. This study has simulated the polymer degradation induced by fast secondary electrons, which are formed in the track of highly energetic GCRs penetrating a material, by irradiating PMMA and Kapton with 5 keV electrons. In LEO, atomic oxygen particles are completely stopped by a 3.5 nm protective layer of aluminium oxide deposited on a polymer surface.<sup>38</sup> However, 5 keV electrons are calculated<sup>12</sup> to lose only about 60 eV of kinetic energy by penetrating through the same protective coating, meaning that 4.94 keV is retained by the impinging electron to sustain damage to the polymer lying beneath the protective coating. In the near-Earth environment this effect is compounded as GCR irradiation consisting of MeV or GeV protons or helium nuclei loses less than 1% of their kinetic energy to the aluminium oxide layer. Therefore in the context of spacecraft design, it is important to discriminate if the spacecraft is operating in LEO, where atomic oxygen is the most abundant form of ionizing radiation and can be effectively stopped by a thin protective coating, or if the spacecraft is operating in deep space such as extended missions to the Moon or mars where GCR irradiation can be problematic. In conclusion, the present study has confirmed that PMMA and Kapton are both susceptible to chemical decomposition by interaction with energetic electrons. Sufficient care must be taken when preparing these materials for aerospace applications as the integrity of the polymers can be compromised by exposure to ionizing radiation in both the LEO and deeper space environments.

## Acknowledgements

This project was supported by Air Force Office of Scientific Research (A9550-09-1-0177). We thank Dr Chris Bennett, UH, for valuable discussions.

## References

- 1 S. M. Pawde and K. Deshmukh, *J. Appl. Polym. Sci.*, 2009, **114**, 2169–2179.
- 2 F. E. Truica-Marasescu and M. R. Wertheimer, *Macromol. Chem. Phys.*, 2005, **206**, 744–757.
- 3 R. Li, C. Li, S. He, M. Di and D. Yang, *Radiat. Phys. Chem.*, 2007, **76**, 1200–1204.
- 4 E. Grossman and I. Gouzman, *Nucl. Instrum. Methods Phys. Res., Sect. B*, 2003, **208**, 48–57.
- 5 K. B. Shin, C. G. Kim, C. S. Hong and H. H. Lee, *Composites, Part B*, 2000, **31**, 223–235.
- 6 A. R. Chambers, I. L. Harris and G. T. Roberts, *Mater. Lett.*, 1996, **26**, 121–131.
- 7 M. L. Everett and G. B. Hoflund, *Macromolecules*, 2004, **37**, 6013–6018.
- 8 E. R. Benton and E. V. Benton, *Nucl. Instrum. Methods Phys. Res., Sect. B*, 2001, **184**, 255–294.
- 9 C. J. Bennett, S. H. Chen, B. J. Sun, A. H. H. Chang and R. I. Kaiser, *Astrophys. J.*, 2007, **660**, 1588–1608.
- 10 J. Cazaux, *J. Phys. D: Appl. Phys.*, 2005, **38**, 2433–2441.
- 11 T. E. Maday, R. E. Johnson and T. M. Orlando, *Surf. Sci.*, 2002, **500**, 838–858.
- 12 D. Drouin, A. R. Couture, R. Gauvin, P. Hovington, P. Horny and H. Demers, Univ. Sherbrooke, Quebec, 2.42 edn, 2002.
- 13 J. Dybal and S. Krimm, *Macromolecules*, 1990, **23**, 1301–1308.
- 14 J. M. O'Reilly and R. A. Mosher, *Macromolecules*, 1981, **14**, 602–608.
- 15 C. J. Bennett, C. S. Jamieson and R. I. Kaiser, *Astrophys. J., Suppl. Ser.*, 2009, **182**, 1–11.
- 16 S. M. Sayyah, M. A. El-Ahdal, Z. A. El-Shafiey, M. El-Sockary and U. F. Kandil, *J. Polym. Res.*, 2000, **7**, 97–106.
- 17 B. D. Silverman, *Macromolecules*, 1989, **22**, 3768–3776.
- 18 H. Ishida, S. T. Wellinghoff, E. Baer and J. L. Koenig, *Macromolecules*, 1980, **13**, 826–834.
- 19 K. Ha and J. L. West, *J. Appl. Polym. Sci.*, 2002, **86**, 3072–3077.
- 20 V. Shrinet, U. K. Chaturvedi, S. K. Agrawal, V. N. Rai and A. K. Nigam, *Polyimides: Synth., Charact., Appl. [Proc. Tech. Conf. Polyimides]*, 1984, **1**, 555–571.
- 21 J. P. LaFemina, G. Arjavalangam and G. Hougham, *J. Chem. Phys.*, 1989, **90**, 5154–5160.
- 22 E. H. Lee, G. R. Rao and L. K. Mansur, *Radiat. Phys. Chem.*, 1999, **55**, 293–305.
- 23 T. M. Hall, A. Wagner and L. F. Thompson, *J. Appl. Phys.*, 1982, **53**, 3997–4010.
- 24 S. A. Sandford, L. J. Allamandola, A. G. G. M. Tielens and G. J. Valero, *Astrophys. J.*, 1988, **329**, 498–510.
- 25 S. A. Sandford and L. J. Allamandola, *Astrophys. J.*, 1990, **355**, 357–372.
- 26 K. H. Heffner, *PhD Thesis*, Univ. of South Florida, 2003.
- 27 J. I. Steinfeld, J. S. Francasco and W. L. Hase, *Chemical Kinetics and Dynamics*, Prentice-Hall, New Jersey, 1989.
- 28 S. Y. Chiang, Y. C. Hsu and Y. P. Lee, *J. Chem. Phys.*, 1989, **90**, 81–86.
- 29 A. Snelson, *J. Phys. Chem.*, 1970, **74**, 537–544.
- 30 H. S. Virk, *Nucl. Instrum. Methods Phys. Res., Sect. B*, 2002, **191**, 739–743.
- 31 Y. Sun, Z. Zhu and C. Li, *Nucl. Instrum. Methods Phys. Res., Sect. B*, 2002, **191**, 805–809.
- 32 G. Peng, W. Hao, D. Yang and S. He, *J. Appl. Polym. Sci.*, 2004, **94**, 1370–1374.
- 33 T. Steckenreiter, E. Balanzat, H. Fuess and C. Trautmann, *J. Polym. Sci., Part A: Polym. Chem.*, 1999, **37**, 4318–4329.
- 34 A. Sharma, N. L. Singh, M. S. Gadkari, V. Shrinet and D. K. Avasthi, *J. Macromol. Sci., Pure Appl. Chem.*, 2005, **A42**, 149–155.
- 35 D. Severin, W. Ensinger, R. Neumann, C. Trautmann, G. Walter, I. Alig and S. Dudkin, *Nucl. Instrum. Methods Phys. Res., Sect. B*, 2005, **236**, 456–460.
- 36 C. J. Bennett, C. S. Jamieson and R. I. Kaiser, *Phys. Chem. Chem. Phys.*, 2009, **11**, 4210–4218.
- 37 C. J. Bennett, C. S. Jamieson and R. I. Kaiser, *Phys. Chem. Chem. Phys.*, 2010, **12**, 4232–4250.
- 38 R. Cooper, H. P. Upadhyaya, T. K. Minton, M. R. Berman, X. Du and S. M. George, *Thin Solid Films*, 2008, **516**, 4036–4039.
- 39 H. Kudoh, T. Sasuga, T. Seguchi and Y. Katsumura, *Polymer*, 1996, **37**, 4663–4665.

- 
- 40 D. M. Ruck, J. Schulz and N. Deusch, *Nucl. Instrum. Methods Phys. Res., Sect. B*, 1997, **131**, 149–158.
- 41 H. W. Choi, H. J. Woo, W. Hong, J. K. Kim, S. K. Lee and C. H. Eum, *Appl. Surf. Sci.*, 2001, **169–170**, 433–437.
- 42 F. Schrempel, Y. S. Kim and W. Witthuhn, *Appl. Surf. Sci.*, 2002, **189**, 102–112.
- 43 S. O. Cho and H. Y. Jun, *Nucl. Instrum. Methods Phys. Res., Sect. B*, 2005, **237**, 525–532.
- 44 M. Iwata, *Nucl. Instrum. Methods Phys. Res., Sect. B*, 2008, **266**, 3071–3074.
- 45 R. Li, C. Li, S. He, M. Di and D. Yang, *Radiat. Phys. Chem.*, 2008, **77**, 482–489.